Transition path sampling of cavitation between molecular scale solvophobic surfaces

Cite as: J. Chem. Phys. **113**, 8154 (2000); https://doi.org/10.1063/1.1315997
Submitted: 15 June 2000 • Accepted: 16 August 2000 • Published Online: 31 October 2000

Peter G. Bolhuis and David Chandler

Transition path sampling of cavitation between molecular scale solvophobic surfaces

Peter G. Bolhuis
Department of Chemistry, University of Cambridge, Cambridge CB21EW, United Kingdom

David Chandler[a)]
Department of Chemistry, University of California, Berkeley, California 94720

(Received 15 June 2000; accepted 16 August 2000)

The dynamics of a cavitation transition between repulsive plates in a Lennard-Jones system is studied using transition path sampling. It is found that the critical nucleus for the transition coincides with the formation of a vapor tube connecting the two plates. The number of particles between the plates and the tube radius are relevant order parameters. In the transition state ensemble, the distributions of these parameters have widths that are roughly 20% of their respective means. Committor distributions of constrained ensembles show that of these two important parameters, the tube radius is the most significant component in the reaction coordinate for the cavitation transition. © *2000 American Institute of Physics.* [S0021-9606(00)52042-X]

I. INTRODUCTION

A liquid that is thermodynamically stable in the bulk, can become metastable with respect to the vapor phase when confined between two hard or repulsive walls. When the walls are close enough to each other, cavitation occurs, and the liquid evaporates.[1] This transition, akin to drying, may explain solvophobic (e.g., hydrophobic) attractions.[2–7] Such interactions are believed to play a central role in the formation and stability of mesoscopic assembly, including biological structures.

For large solvophobic surfaces, macroscopic arguments apply, and one can make an estimate for the critical separation, D_c, at which the liquid is destabilized against the vapor. The liquid film has an unfavorable surface energy proportional to the net surface area. This energy is opposed by the favorable bulk free energy which is proportional to the difference in chemical potential between the gas and the liquid. For large separation D the bulk free energy dominates and the liquid film is stable. If D is of the order

$$D_c \sim \frac{2\gamma}{n_l \mu_{lg}}, \tag{1}$$

where γ is the surface tension, n_l is the liquid density and μ_{lg} the difference between gas and liquid chemical potentials. When the fluid is relatively close to liquid–gas coexistence, this critical distance can be quite large on a molecular scale. For instance, for water at ambient conditions $D_c \approx 100\,\text{nm}$.

For smaller surfaces down to the nanometer length scale, the same qualitative reasoning applies, although the critical distance will be smaller. In contrast, for very small solutes, solvophobic particles of the same size as the solvent molecules, drying is not observed. Attractive interactions between solvent molecules, manifested for example in surface tension, can accommodate a very small solute without much loss of adhesive energy. According to the theory of Lum, Chandler, and Weeks,[2] the crossover to the drying regime occurs for solvophobic surfaces that extend over a few correlation lengths. For example, hard spheres in water induce solvent density depletion when the sphere radii are about 1 nm or larger.[2] Hard spheres in the Lennard-Jones liquid near its triple point induce similar depletion when the sphere radii are larger than about 2.5σ, where σ is the usual Lennard-Jones particle diameter.[8]

The first simulation of a drying (also called cavitation) transition between two repulsive walls was done by Benard, Attard, and Patey,[3] although earlier work exists on drying at a single wall. These authors studied the equilibrium properties of the first order transition by Monte Carlo methods. Drying of surfaces immersed in water and the resulting hydrophobic force was observed in a computer experiment by Wallqvist and Berne[9] using molecular dynamics. Subsequently, Forsman *et al.*[4–7] focused on the relation between hydration and hydrophobic forces in water using isotension and grand canonical simulation. Since then, a few other theoretical studies have been performed using simple liquid models with Lennard-Jones-type interactions.[10,11]

There are fewer studies of the dynamics of this transition. Lum and Luzar studied a drying transition between solvophobic plates in a lattice gas by employing Glauber dynamics.[12] They concluded that the transition is driven by surface fluctuations. Subsequent analytical work identified a reasonable reaction path and estimated the activation free energy for this drying of a semi-infinite slab.[13] Until the work we report on now in this paper, no continuous off-lattice fluid model has been used to study the dynamics of the drying transition. The absence of such work is not surprising since in general, the drying transition is a rare event. As such, a straightforward dynamical simulation is generally infeasible. A standard way to study the dynamics of rare events is the application of the reactive flux method.[14] This

[a)]Electronic mail: chandler@cchem.berkeley.edu

method requires *a priori* knowledge of a physically reasonable reaction coordinate. However, for the finite solvophobic plate system considered here, the reaction coordinate is not known. As such, application of the reactive flux method for this situation can be misleading. To overcome this problem, we use the method of transition path sampling, recently developed by the authors and their coworkers.[15–18] Transition path sampling enables one to harvest an ensemble of trajectories that connect one basin of attraction with another. The algorithm requires no preconceived notion of mechanisms or transition states.

We investigate the drying transition between two repulsive plates in a Lennard-Jones fluid. The principle aim of this paper is twofold. Firstly, to show that it is possible to study this type of first-order like transitions with high activation barriers using the transition path sampling method. Secondly, to establish a proper reaction coordinate for the cavitation transition. A first candidate for a reaction coordinate for the cavitation transition is the distance between the plates. However, the transition also occurs for surfaces at a fixed distance.[3] Clearly, the reaction coordinate must involve another parameter. The next likely candidate is the density of the fluid between the plates, which is low in the case of a vapor and high for a liquid film. As we show in this paper, this order parameter does not describe the full dynamics either. The transition occurs via a nucleation mechanism, creating a tube of vapor connecting the two surfaces that grows into a vapor layer. By computing the committor distributions for constrained ensembles,[19,20] we demonstrate that the size of the vapor nucleus is most likely the correct reaction coordinate for the cavitation transition.

Note that the drying transition is strictly only a phase transition in the thermodynamic limit, for macroscopic surfaces. In this paper, we use the term phase transition also for finite systems. This terminology is very tempting, as the characteristics of the transitions are much akin to macroscopic first-order phase transitions, including the mechanism of nucleation.

This paper is organized as follows. In the next section we describe the model system we use to study the drying transition. Subsequently, we discuss the computed force between the two surfaces as a function of their distance. The results indicate a collective density depletion, akin to a first-order phase transition, takes place for plates at a fixed distance. Section IV focuses on this cavitation transition between two plates at fixed distance. In Sec. V, we investigate the dynamics of this transition by transition path sampling. The path ensemble is subsequently analyzed by determining the transition state ensemble. In Sec. VII, the validity of several order parameters is tested by computing committor distributions. We end with concluding remarks.

II. MODEL

We studied the drying transition between two repulsive plates in a truncated and shifted Lennard-Jones (LJ) fluid. The pair potential between the fluid particles is given by

$$v(r)=\begin{cases}\phi(r)-\phi(R_c) & \text{if } 0\leqslant r\leqslant R_c\\ 0 & \text{if } r>R_c\end{cases}. \tag{2}$$

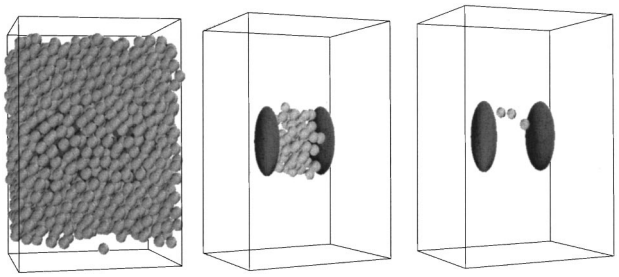

FIG. 1. The system consists of a truncated and shifted LJ fluid between two repulsive walls (external field). The system is periodic in the x and y direction. The outer walls dry at low temperatures and a stable liquid film is formed between the outer walls (left picture). Inside the fluid two repulsive (solvophobic) plates are placed. For clarity, the middle figure shows only the small plates and the liquid layer in between. The region between these plates is where the cavitation takes place. In the right panel the liquid has evaporated.

Here, r is the interparticle distance, $R_c=2.5\sigma$ is the cut-off radius, and $\phi(r)$ is the usual Lennard-Jones potential

$$\phi(r)=4\epsilon\left[\left(\frac{\sigma}{r}\right)^{12}-\left(\frac{\sigma}{r}\right)^{6}\right], \tag{3}$$

where ϵ is the depth of the potential and σ is the diameter of the particles.

As we are interested in the *dynamics* of the cavitation or drying transition, it is not possible to use simulation techniques in which only the fluid between the two plates is simulated, such as grand canonical or isotension algorithms.[1,3,4] We have to allow for the fluid to diffuse out of the space between the plates. Therefore, we instead chose the system setup shown in Fig. 1. Two circular plates with a radius of 3σ each are immersed in a LJ fluid and interact via the purely repulsive Weeks–Chandler–Andersen (WCA) potential with the solvent particles. The WCA potential is given by

$$v_{\mathrm{WCA}}(r)=\begin{cases}\phi(r)+\epsilon & \text{if } r\leqslant r_{\mathrm{WCA}}\equiv 2^{1/6}\sigma\\ 0 & \text{if } r>r_{\mathrm{WCA}}\end{cases}. \tag{4}$$

The WCA potential acts along the line of shortest distance between the center-of-mass of the LJ particles and the plate. The size of the plates is large enough to exhibit drying.[8] Taking 2 Å σ 4 Å, the plates are of the same length scale as hydrophobic surfaces of biomolecules in aqueous solution. For simplicity, the plates remain parallel, perpendicular to the x axis and are only allowed to move along the x axis.

Due to the expected cavitation, the density outside the plates and, therefore, the total pressure is likely to increase. Therefore, a constant pressure simulation is required. Applying a Nose–Hoover chain[21] in order to create a constant pressure and temperature ensemble is unphysical for this application because it artificially changes the volume. Instead, we ensured constant pressure by dressing two opposite walls of the simulation box with a repulsive WCA potential. At conditions sufficiently close to the triple point, the outer walls dry and vapor–liquid coexistence is established. If the simulation box is large enough, the liquid film will be stable and

show near bulk behavior. Inside this stable liquid, the two plates are put perpendicular to the outside walls to have minimal impact of lateral fluctuations.

In all simulations we employed the Lennard-Jones potential, truncated at 2.5σ and subsequently shifted to obtain a continuous potential. The plates and the outer walls are made repulsive with a WCA potential. Throughout the paper we use the standard reduced Lennard-Jones units, i.e., length is measured in units of σ, energies in units of ϵ, time in units of $\tau=(m\sigma^2/\epsilon)^{1/2}$. The systems consisted of 2000 particles in a box with sides of length 13.9629σ, 11.9682σ, and 19.9469σ for the x, y, and z dimensions, respectively. The z dimension was chosen longer to ensure a reasonably thick liquid layer that would exhibit near bulk behavior. The overall number density was $\rho\sigma^3=0.6$. In the molecular dynamics (MD) simulations we used a time step $\Delta t=0.01\tau$.

III. FORCE BETWEEN PLATES

We calculated the average force, f, between the plates as a function of the distance D between the plates. In a microcanonical MD simulation the plates were constrained at a fixed distance. The system was then equilibrated for 10 000 time steps, after which the forces on the plates were measured for a duration of 10 000 time steps. Subsequently, the inter plate distance was changed by 0.2σ and the force was measured again. In this way we obtained the full force curves for both compressing (bringing the plates closer together) and expanding. The cycle of compression and expansion between $D/\sigma=3.6$ and $D/\sigma=6.4$ was repeated about 10 times, to obtain better statistics. The force curves are shown in Fig. 2 for the reduced temperatures $T^*\equiv k_BT/\epsilon=0.81$, 0.67, and 0.58 ($k_B$ denotes Boltzmann's constant). The temperature of the system was imposed by adjusting the total energy of the system. All curves show a zero force at large plate separation, which corresponds to a stable liquid film between the plates. At smaller separation the vapor phase becomes stable, causing a pressure imbalance that results in the net attractive force.

The upper panel of Fig. 2 represents the highest temperature case and shows no hysteresis between the compression and expansion curves. The middle panel already has a small amount of hysteresis. In contrast, the force curve for the lowest temperature, where $T^*=0.58$, is shown in the lower panel of Fig. 2, and exhibits a large amount of hysteresis, suggesting that even for a fixed distance between the plates, density depletion, or cavitation will occur in a fashion akin to a first order transition between a liquid film and a vapor. The lowest temperature is still above the triple point temperature. The triple point temperature for the truncated and shifted Lennard-Jones model we use here is approximately at $k_BT/\epsilon\approx0.55$. We estimated this value by determining the point of intersection of the vapor liquid coexistence curve with the fluid solid line. The vapor–liquid coexistence was obtained by extrapolation of the Gibbs Ensemble Monte Carlo simulation results by Smit.[22] The solid-fluid coexistence curve was estimated by taking the Gibbs Duhem integration results of Agrawal and Kofke[23] for the regular Lennard-Jones system and assuming that the shifting and truncating will shift the temperature slightly downwards, but will not change the phase behavior drastically.

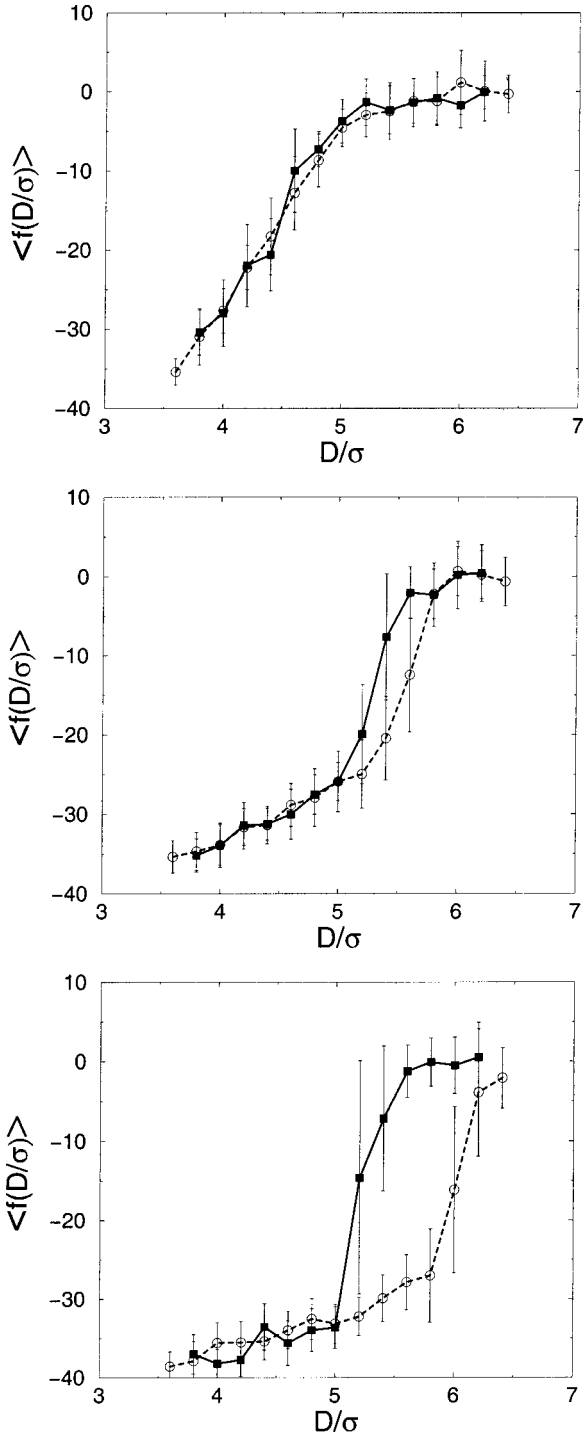

FIG. 2. Forces between the two plates as a function of their distance for different temperatures. Open circles denote the expansion cycle, closed squares denote a compression.

IV. FIXED PLATE DISTANCE

Before embarking on the transition dynamics for moving plates, we studied the drying transition in system with fixed plates. In this case, an obvious order parameter characterizing the basins of attraction is the bulk particle density between the plates, which is high in the liquid phase and low in

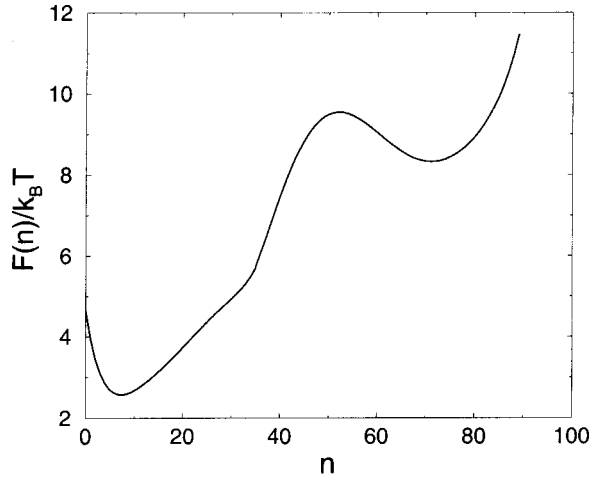

FIG. 3. Free energy for a fixed plate distance $D/\sigma=5.6\sigma$ at $T^*=0.58$ as a function of the particle density between the plates. The free energy curve has two minima. The minimum at low n corresponds to the vapor phase, which is the most stable in this situation. The liquid phase between the plates is metastable.

the vapor. As the system is of finite size, we specify this density with the total number of particles, n, between the two plates. Conversion to the density is easily done by dividing by the volume between the plates. The free energy as a function of the density or number of particles is informative. It is

$$F(n)=-k_BT\ln[P(n)], \tag{5}$$

where $P(n)$ is the probability to find n particles between the plates.

We performed Monte Carlo umbrella sampling[24] for the Lennard-Jones system described in Sec. II with a fixed plate distance of 5.6σ and a temperature $T^*=0.58$. These values corresponds to a large hysteresis in the force curves. Five windows were sampled, $0\leqslant n\leqslant 20$, $20\leqslant n\leqslant 40$, $30\leqslant n\leqslant 50$, $45\leqslant n\leqslant 65$, and $60\leqslant n\leqslant 90$. The system was not allowed to sample outside a window. The sampling was biased to obtain a flat distribution in each window for optimal statistics. The free energy curve was estimated by matching the histograms for each window and applying Eq. (5). The free energy as a function of n is shown in Fig. 3. It clearly shows two stable states separated by a barrier. The liquid film turns out to be metastable, as one would expect for a small interplate distance. The plates are repulsive, and the vapor–liquid coexistence will shift to lower temperature, so the gas phase will be stabilized. Were we to think that the order parameter n is also a good approximation to a reaction coordinate, the barrier shown in Fig. 3 would seem rather low. Straightforward molecular dynamics indicate that the system stays in the liquid film state for a considerable time, $t>100\tau$. (The time will be even longer for solvophobic surfaces with larger areas at larger distances.) The apparent low barrier found for $F(n)$ is evidence that another variable in addition to n is needed to describe the dynamics of the transition.

V. TRANSITION PATH SAMPLING

The method of transition path sampling enables one to collect trajectories connecting two stable regions A and B with a Monte Carlo algorithm called ''shooting.''[16,17] In this algorithm, one randomly chooses a particular configuration on an existing initial trajectory and changes the momenta slightly. By integrating the equations of motion forward and backward in time one obtains a new trial path. If the trajectory still connects A with B the Monte Carlo shooting move is accepted and one replaces the old path with the trial. If it fails to connect A with B, the trial path will be rejected. In this way one can sample trajectory space and obtain dynamical information from an ensemble of pathways. For the cavitation transition, we defined the initial state by $n>60$ (the liquid film) and the final state by $n<30$ (the vapor phase). These values are chosen such that even at the boundaries of a stable state, the system is completely committed to the basin of attraction of that stable state. The stable liquid and vapor states are denoted L and G, respectively. An initial path was obtained by shooting from the top of the barrier obtained by umbrella sampling of n. A workable trajectory was only found after a considerable amount of trial shoots, indicating that the transmission coefficient is low. Such a low value suggests that the order parameter n is not a good description for the reaction coordinate.

The length of the trajectories used in the path sampling simulations was $\mathcal{T}=80\tau$. Every 0.8τ a configuration was saved, resulting in a total of 100 time slices per trajectory. The number of attempted shoots was 2000 of which 15% was accepted. The number of shifting moves[17] was 2000 with an acceptance ratio of 60%. We also applied 50 000 small shifts of one time slice each to obtain better statistics in the time correlation functions. The path sampling simulations were done in the microcanonical ensemble. The total energy was kept constant at $E=-8000\epsilon$, which roughly corresponds to a temperature of $T^*=0.58$.

The reactive flux time correlation $\langle h_L(0)h_G(t)\rangle$ can be used to check if representative paths are harvested by the sampling.[16] The characteristic function $h_A(t)$ for stable state A is defined as

$$h_A(t)=\begin{cases}1 & \text{if } n(t)\in A\\ 0 & \text{if } n(t)\notin A\end{cases}, \tag{6}$$

where $n(t)$ is the number of particles between the plates at a time t along the trajectory. The pointed brackets indicate an ensemble average over trajectories. If this correlation function reaches a linear regime the trajectories are long enough to incorporate most of the dynamical pathways. If this criterion is not fulfilled, path sampling should consider longer trajectories. The reactive flux $\langle h_L(0)h_G(t)\rangle$ and its time derivative were calculated during the path sampling simulation. A plateau in the time derivative of $\langle h_L(0)h_G(t)\rangle$ is reached for $t>60\tau$, showing the path length is sufficiently long.

In principle, it is possible to extract rate constants from path ensembles using an umbrella sampling technique.[16–18] This technique is the most computationally intensive part of transition path sampling. Since this study is only concerned with the qualitative nature of the drying transition dynamics, we have not performed quantitative rate constant calculations.

To reveal the mechanism of the transition, we plot a typical trajectory as a sequence of configurations in Fig 4.

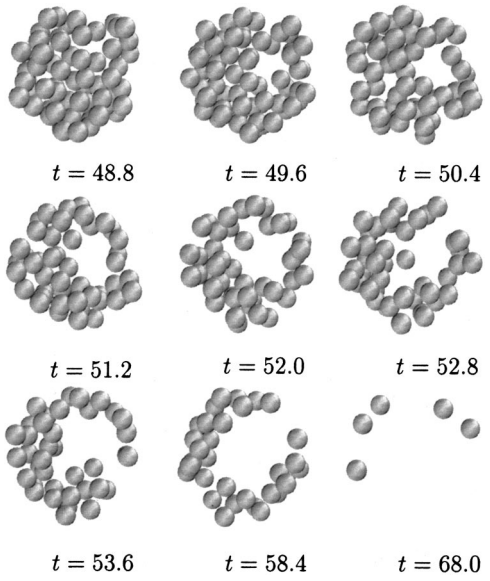

FIG. 4. Typical pathway as obtained from the transition path sampling. Only the region between the plates is shown. The times are given in units of τ from the start of the trajectory. The configuration at the center is the transition state for this trajectory.

For clarity, only the region between the two hydrophobic plates is depicted and the plates themselves are not shown. The sequence shows the formation of a gas bubble between the two plates which grows into a vapor layer. This suggests that the transition from the liquid to the vapor takes place via a nucleation of a critical vapor nucleus. Consistent with this mechanism, in some trajectories, we find the formation of subcritical vapor bubbles that subsequently disappear.

VI. TRANSITION STATE ENSEMBLE

One of the ways to analyze transition path sampling results is by determining the transition state ensemble (TSE) from the path ensemble. The TSE can be obtained with the method described in Refs. 17 and 25. For every time slice on a path one calculates the so-called committors, p_G and p_L. These quantities are the probabilities that trajectories initiated from that configuration will quickly flow, respectively, to gaslike or liquidlike configurations. A configuration for which $p_G = p_L$ is considered a member of the transition state ensemble (TSE). We have found such members of the TSE by initiating 50 trajectories for every time slice. The length of each trajectory was 40τ.

In order to visualize the TSE, one can calculate several distribution functions. The upper panel of Fig. 5 shows the distribution of the number of particles between the plates, n, for the TSE. The variation in the number of particles is not small, indicating the importance of another variable in the kinetics. Upon inspection, we have found that all TSE configurations exhibit a gas bubble between the two plates. This finding suggests the importance bubble size. The vapor bubble size in the TSE corresponds to a critical nucleus size. We estimated the size of the vapor nucleus by determining the largest cylinder with a radius r_b perpendicular to the plates that fits in the bubble without overlapping with any of the fluid particle's center-of-mass. The distribution of the bubble size is shown in the lower panel of Fig. 5. The bubble size distribution has an average of $r_b = 1.3\sigma$, and a standard deviation of 0.2σ. The relative standard deviation is larger than that of n in the TSE, but the distribution in this case is smoother. Figure 6 shows the harvested members of the TSE projected onto the $n - r_b$ plane. It is clear that both variables, n and r_b, are important in the kinetics.

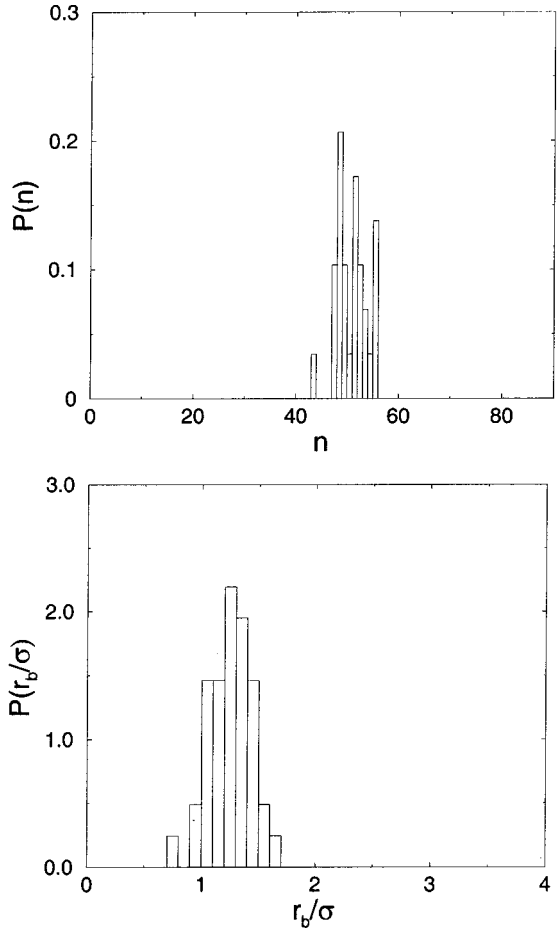

FIG. 5. Top: Distribution of the density in the TSE. Bottom: Distribution of the bubble radius in the TSE.

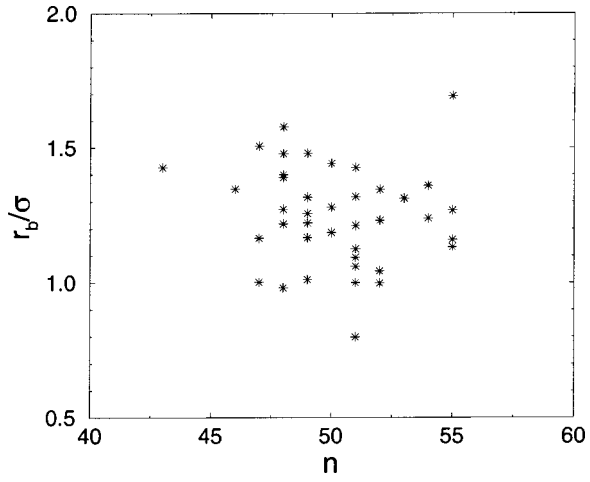

FIG. 6. Members of the TSE in the $r_b/\sigma - n$ plane.

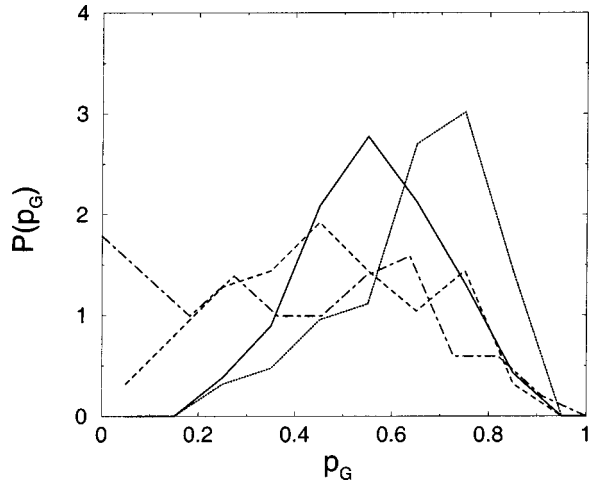

FIG. 7. Distribution of the committor p_G for constrained ensembles $n=49$ (dotted line), $n=50$ (dashed line) and $n=51$ (dot-dashed line). The distribution of the committor p_G for a constrained ensemble with $r_b/\sigma=1.28$ is shown as a solid line.

VII. COMMITTOR DISTRIBUTION

The validity of a variable ξ in describing the reaction coordinate can be checked by computing the probability distribution of the committor, p,[19,20] for an ensemble in which ξ is constrained to a certain value. This distribution, $P(p;\xi)$, gives information about how important other degrees of freedom are. For example, a distribution that is peaked around $p=0.5$ indicates that ξ describes the transition rather well, whereas a distribution peaked at $p=0$ and $p=1$ suggests that there is an additional barrier orthogonal to ξ.[19]

We calculated the distribution $P(p_G;n)$ for the drying transition for three constrained ensembles: $n=49$, $n=50$, and $n=51$. The constrained ensembles were generated by Monte Carlo simulation. The ensemble consisted of 200 configurations for each ensemble. For every configuration we initiated 50 trajectories with momenta drawn from a Gaussian distribution. The total energy was again fixed to $E=-8000\epsilon$. The length of each trajectory was 40 LJ time units. The results are plotted in Fig. 7. The $P(p_G;n)$ distribution is broad for all three ensembles. For $n=51$ its average is around $p_G=0.3$, indicating that the system is more likely to go to the metastable liquid state. For the $n=49$ ensemble the distribution is shifted to higher p_G values, corresponding to a higher probability to end up in the vapor phase. The committor for the $n=50$ ensemble is also broadly distributed, but it is peaked around $p_G=0.5$. All three distributions are peaked around a value close to $p_G=0.5$. This finding suggests that a barrier associated with another parameter is likely to be small.

We also computed the committor distribution for the radius of the vapor nucleus, to test the validity of the bubble radius as a reaction coordinate. A constrained ensemble was constructed by Monte Carlo simulation for a bubble radius of $r_b=1.28\sigma$ which corresponds to the maximum of the distribution in Fig. 5 with the same conditions as above. The committor distribution for this ensemble is also shown in Fig. 7. It is peaked around $p_G=0.5$ and narrower than the corresponding distribution for the density. This result indicates again that the bubble size is a good reaction coordinate. On the basis of nucleation theory,[13] we expect this result to hold for larger solvophobic surfaces, whereas we expect the committor distribution for n to become flatter and even bimodal for larger solvophobic surfaces.

VIII. CONCLUSION

A cavitation transition of a Lennard-Jones liquid between two repulsive surfaces takes place by nucleation of a vapor bubble between the surfaces. First, a vapor bubble has to be formed by fluctuations connecting the two surfaces. This bubble has to be of a critical size before it can grow to a full vapor layer. This critical vapor nucleus is the transition state.

The committor distributions indicate the same trend more clearly. The committor distribution for the radius of the nucleus is sharper peaked around $p_G=0.5$ than the corresponding distribution for the density. For larger plates, this trend will be more pronounced.

A possible extension of this work involves the inclusion of moving plates. In that case the plates still have to overcome a barrier, because a nucleus has to be formed, but the distance between the plates clearly plays an additional role. Allowing the plates to move, may well lower the barrier.

The cavitation transition in a LJ fluid acts as a simple model for the hydrophobic effect. An important question is if the mechanism observed here is the same for hydrophobic surfaces in aqueous solution. And if so, how large is the barrier that has to be overcome, if there is a substantial barrier at all.

A more general conclusion of the current work is that we have demonstrated that it is in principle possible to study the dynamics of first order (although of finite system size) phase transitions using the path sampling method. Other applications that involve dynamics of first order transitions, such as the nucleation of a crystal in the melt, thus come within reach of being investigated without imposing a preconceived reaction coordinate.

ACKNOWLEDGMENTS

P.B. and D.C. are grateful for the financial support by Office of Basic Energy Sciences, Chemical Sciences Division of the U. S. Department of Energy under Contract No. DE-FG03-99ER14987.

[1] R. Evans, J. Phys.: Condens. Matter **2**, 8989 (1990).
[2] K. Lum, D. Chandler, and J. D. Weeks, J. Phys. Chem. B **103**, 4570 (1999).
[3] D. R. Berard, P. Attard and G. N. Patey, J. Chem. Phys. **98**, 7236 (1993).
[4] J. Forsman, B. Jönsson, C. E. Woodward, and H. Wennerström, J. Phys. Chem. B **101**, 4253 (1997).
[5] J. Forsman, B. Jönsson, and C. E. Woodward, J. Phys. Chem. **100**, 15005 (1996).
[6] J. Forsman, C. E. Woodward, and B. Jönsson, J. Colloid Interface Sci. **195**, 264 (1997).
[7] J. Forsman and B. Jönsson, J. Chem. Phys. **101**, 5116 (1994).
[8] D. M. Huang and D. Chandler, Phys. Rev. E **61**, 1501 (2000).
[9] A. Wallqvist and B. J. Berne, J. Phys. Chem. **99**, 2893 (1995).
[10] H. Dominguez, M. P. Allen, and R. Evans, Mol. Phys. **96**, 209 (1999).
[11] C. Bruin, Physica A **251**, 81 (1998).
[12] K. Lum and A. Luzar, Phys. Rev. E **56**, R6283 (1997).

[13] K. Lum and D. Chandler, Int. J. Thermophys. **19**, 845 (1998).
[14] See, for example, C. H. Bennett, in *Algorithms for Chemical Computations, ACS Symp. Ser. No. 46*, edited by R. E. Christofferson (American Chemical Society, Washington, 1977), p. 63; and D. Chandler, J. Chem. Phys. **68**, 2959 (1978); Related and earlier work has been discussed in a brief history communicated by D. Chandler, Faraday Discuss. Chem. Soc. **85**, 341 (1988).
[15] C. Dellago, P. G Bolhuis, F. S. Csajka, and D. Chandler, J. Chem. Phys. **108**, 1964 (1998).
[16] C. Dellago, P. G Bolhuis, and D. Chandler, J. Chem. Phys. **108**, 9236 (1998).
[17] P. G Bolhuis, C. Dellago, and D. Chandler, Faraday Discuss. Chem. Soc. **110**, 421 (1998).
[18] C. Dellago, P. G. Bolhuis, and D. Chandler, J. Chem. Phys. **110**, 6617 (1999).
[19] P. Geissler, C. Dellago, and D. Chandler, J. Phys. Chem. B **103**, 3706 (1999).
[20] P. G. Bolhuis, C. Dellago, and D. Chandler, Proc. Natl. Acad. Sci. U.S.A. **97**, 5877 (2000).
[21] S. Nose, J. Chem. Phys. **81**, 511 (1984); W. G. Hoover, Phys. Rev. A **31**, 1695 (1985).
[22] B. Smit, *Simulation of phase coexistence: from atoms to surfactants*, Ph.D. thesis, University of Utrecht (1990).
[23] R. Agrawal and D. A. Kofke, Mol. Phys. **85**, 43 (1995).
[24] D. Frenkel and B. Smit, *Understanding Molecular Simulations* (Academic, New York, 1995).
[25] P. Geissler, C. Dellago, and D. Chandler, Phys. Chem. Chem. Phys. **1**, 1317 (1999).